Supporting information to

Morphology and Orientation Change of Layer-by-Layer Deposited One- and Two-Dimensional Coordination Polymer Nanocrystals Containing Rhodium Paddle-Wheel Units

Daniel Steinbach,[1†] Richard Neubert,[1†] Sophie Gersdorf,[1] Christian Schimpf,[2] Denise Erb,[3] David Rafaja,[2] Felix A. Plamper, [1,4,5] Florian Mertens[1,4]**

[1]Institute of Physical Chemistry, TU Bergakademie Freiberg, Leipziger Str. 29, 09599 Freiberg, Germany

[2]Institute of Materials Science, Technical University Bergakademie Freiberg, Gustav Zeuner Str. 5, 09599 Freiberg, Germany

[3]Institute of Ion Beam Physics and Materials Research, Helmholtz-Zentrum Dresden-Rossendorf HZDR, 01328 Dresden, Germany

[4]Center for Efficient High Temperature Processes and Materials Conversion ZeHS, TU Bergakademie Freiberg, Winklerstr, 5, Freiberg, 09599 Germany

[5]Freiberg Center for Water Research ZeWaF, TU Bergakademie Freiberg, Winklerstr, 5, Freiberg, 09599 Germany

Supporting Information

Reflectivity of $[Rh_2(ac)_4(pyz)]_n$ deposits

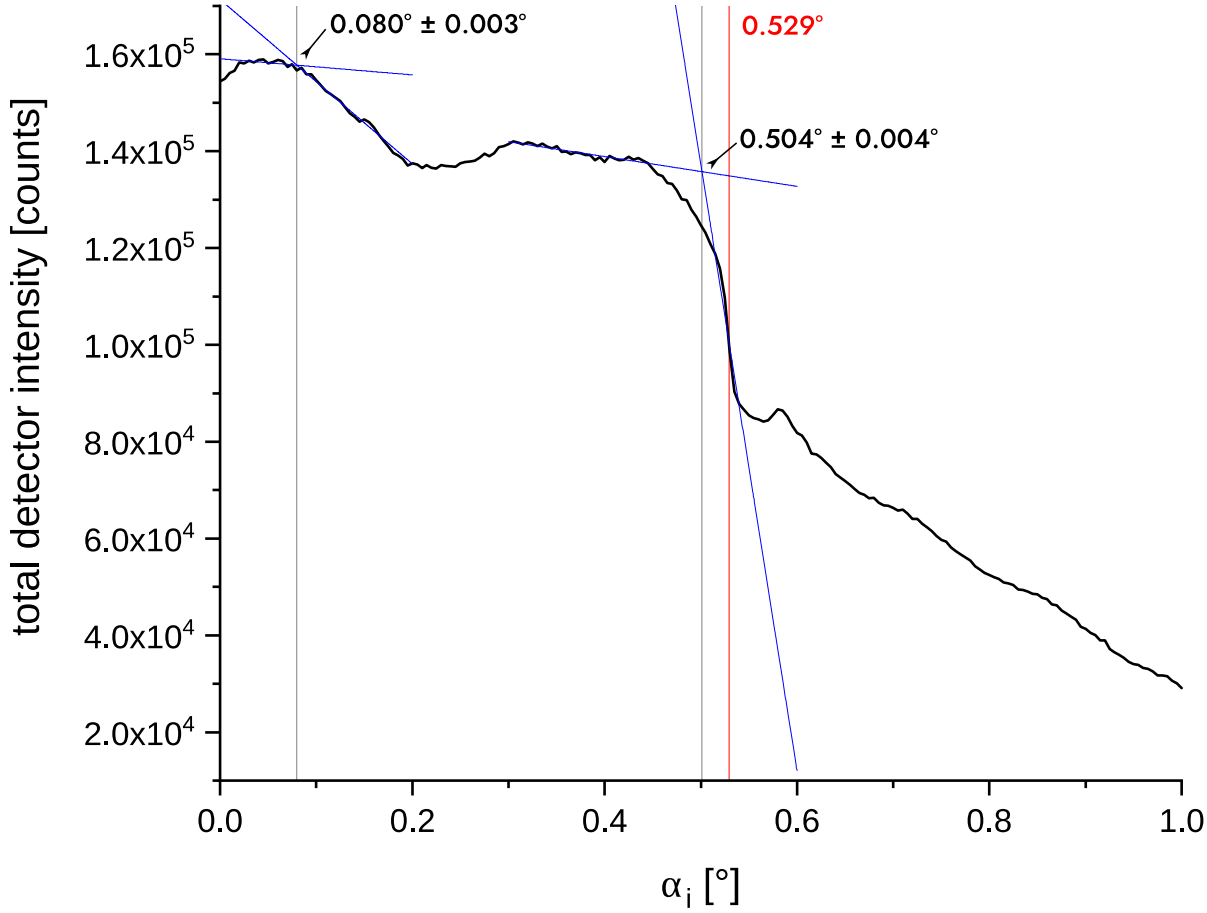

Figure 1: Total intensity hitting the whole detector plane standing perpendicularly 1.62 m behind the illumination spot of the sample within 0.5 s plotted versus the inclination angle; Two distinct critical angles have been identified by determining the intersection between the linear fits of the intensity edge and the preceding plateau.[1]

If the absorption is assumed to be negligible, the SLD (scattering length density) of the coordination polymer deposit can be estimated from the reflectivity pattern: The critical vector q_c relates to the SLD by $q_c = \sqrt{16\pi \cdot SLD}$. Hence, the critical angle can be calculated by

$$\alpha_c = \arcsin\left(\frac{q_c \cdot \lambda}{4\pi}\right) \approx \sqrt{\frac{\lambda^2 \cdot SLD}{\pi}}.$$

According to theory, the angle of total external reflection (TER) of gold should be at 0.529° which is marked in Fig. 1 with a red line. The measured angle for the TER is 0.504°. With this, the (apparent) TER for the decorated gold surface can be corrected and determined to be 0.105°. Then, the SLD of $[Rh_2(ac)_{4(}pyz)]_n$ can be estimated to be about $4.4 \cdot 10^{-6}$ Å^{-2}.[1]

Gold coated Si wafer as substrate

A single crystalline (001) n-doped silicon wafer was treated with 40 % HF to remove the SiO_2 layer. Then, the cleaned wafer was coated by physical vapor deposition (PVD) process with a 5 nm thick titanium layer. Afterwards, the titanium was covered by a 100 nm thick gold layer deposited in a second PVD process.

The wafer was investigated by AFM and GISAXS. The GISAXS pattern in Figure 2 shows two off-specular maxima. Figure 3 displays maxima at -0.064 and 0.064 nm^{-1} in the q_y-cut at the specular peak. These values were derived from the maxima in Fig. 3, after correction of the slightly misaligned position of the specular beam.

This q-spacing represents a real space distance of about 98 nm, which can be interpreted as average distance between the corrugations at the surface. This average distance between two neighbouring centres of gold structures corresponds well to the observed morphology in corresponding AFM images (e.g., Figure 4).

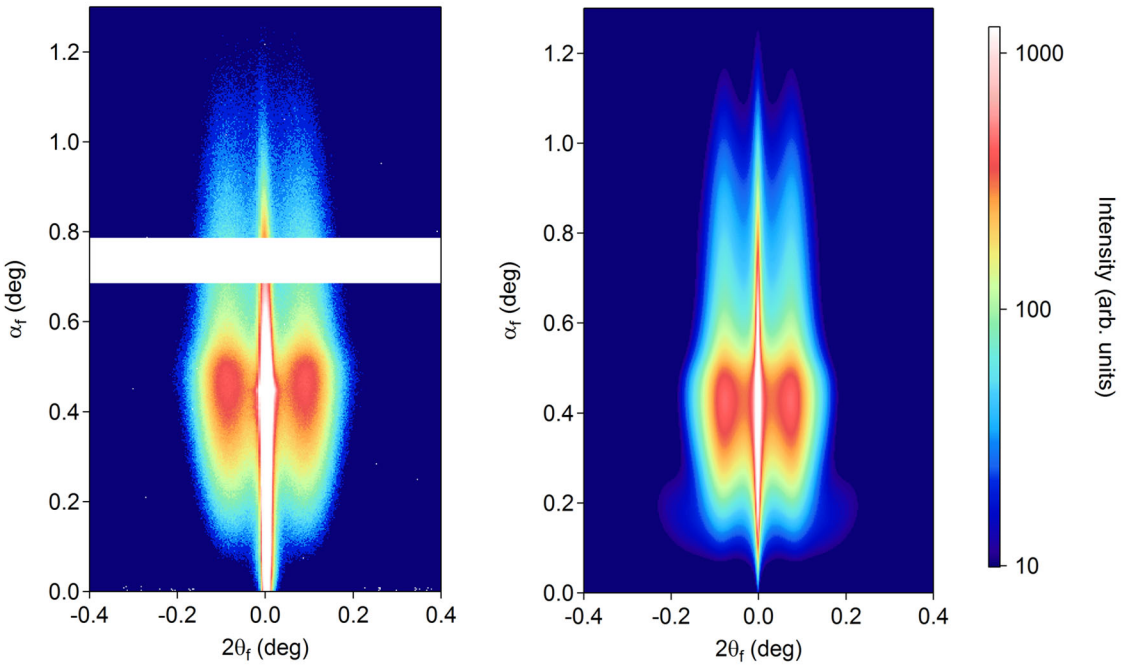

Figure 2: left: GISAXS pattern of clean gold coated Si wafer surface, inclination angle = 0.5° (detector gap visible as stripe); right: simulated pattern with truncated sphere form factor model.

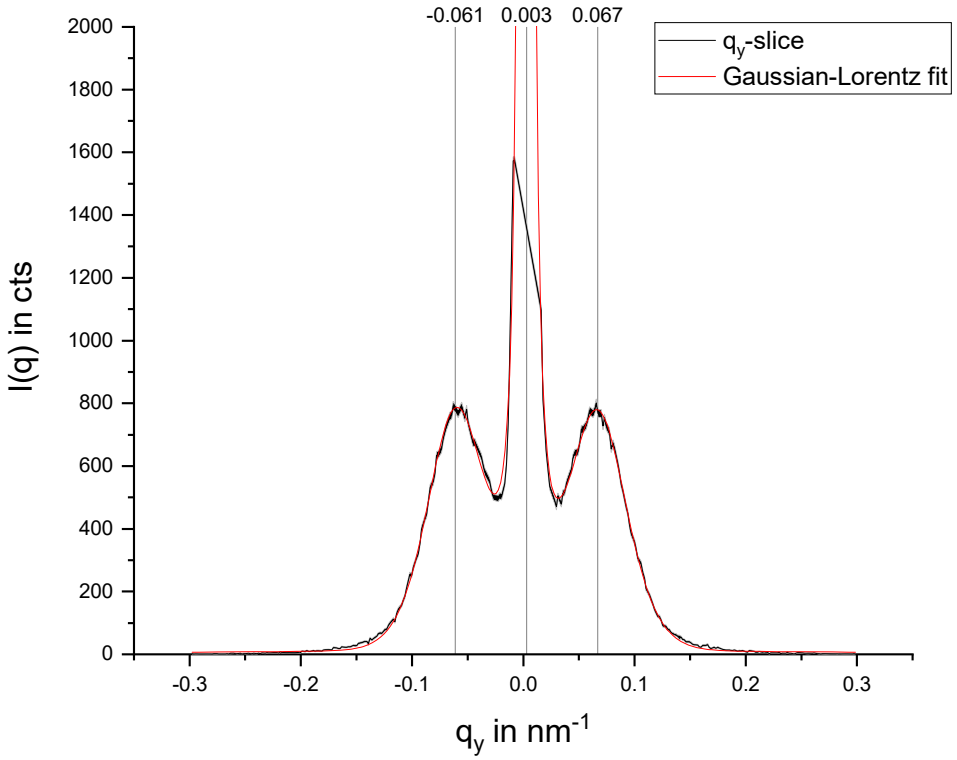

Figure 3: q_y-profile at q_z of the specular peak.

For a more detailed morphology analysis, the GISAXS data were modelled based on the distorted wave Born approximation (DWBA) by means of the software BornAgain.[2] A truncated sphere was used as form factor model with the following parameters:

radius	45 nm
height	10 nm
delta height	0 nm

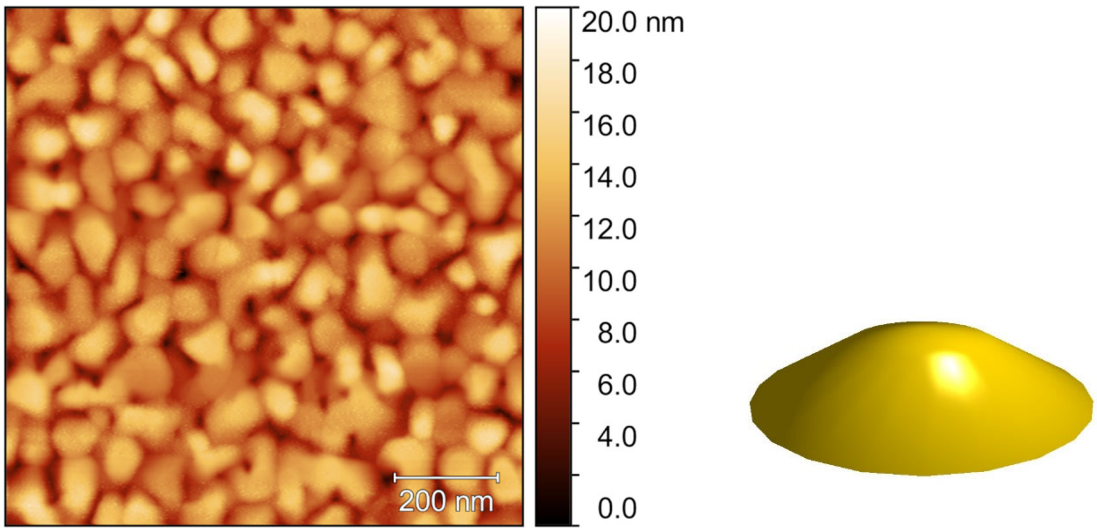

Figure 4: 1 µm x 1 µm AFM picture of gold coated Si wafer with corresponding fitted mean form of a single island (obtained by BornAgain software – see Figure 5).

As it can be seen in the AFM picture in Fig. 4, the gold particles are tapered with a base area which cannot be described well by a rectangular or other simple polygon. Given that GISAXS data represent the average morphological characteristics, choosing the truncated sphere form factor is a pragmatic approach to modelling a sample with a wide variation of particle shapes as observed here. A radial paracrystal model was used to describe the lateral arrangement of the Au particles placed on an Au substrate (placing an Au layer of 100 nm thickness onto a Si substrate in the model instead does not result in any significant changes to the simulated scattering pattern.)

position variance	10 nm
peak distance	85 nm
damping length	750 nm
domain size	2500 nm
size space coupling	1
probability distribution function	Cauchy 1D
omega	30 nm

The resulting distance is in good agreement with the AFM images and smaller than the first evaluation using only the peak maximum. It can be seen that the location of the maximum is only a first hint as it is also described by Renaud and coworkers.[3]

The resulting simulated pattern is in good agreement with the measured pattern, as seen in Fig. 2.

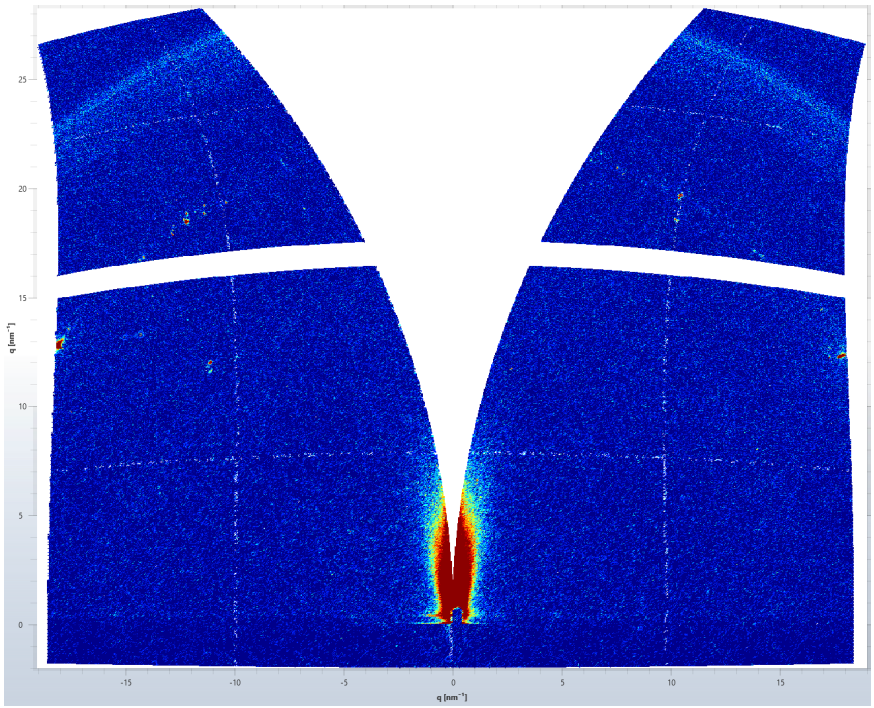

Figure 5: GIWAXS pattern of gold coated Si wafer, inclination angle = 0.3° (detector gap seen as white stripe; q_r-transformation leads to white area in the centre based on the asymmetric position of the detector)

The GIWAXS pattern in Figure 5 of the pure gold coated wafer exhibits the reflection from the (111) plane visible as typical Debye-Scherrer ring at $|\vec{q}| \approx 29nm^{-1}$.

Azimuthal Rotation

The variation of the azimuthal ϕ angle (rotating the sample around the sample surface normal) does not change the position of the (001) reflection maxima significantly, as seen in the detector images of Figure 6. It is also visible in the images that the overall intensity and the scattering near the primary beam changes slightly. This is connected to the roughness of the surface and the inclination of the sample surface from the horizontal direction respectively.

At 45° a small strong reflection maximum at $|\vec{q}| \approx 29nm^{-1}$ becomes visible. Comparing the pattern at 90° and Fig. 5, this Debye-Scherrer ring refers to the gold surface.

In comparison to the initial inclination perpendicular to the dipping direction there is a more intense scattering at ϕ=60° visible. Here the influence of the crystal orientation is visible because different crystal slides are oriented to the beam. Furthermore, at this angle the beam covers partly the meniscus area from the dipping process. The crystals there are not as good oriented as at other positions on the wafer. This could lead to a more isotropic orientation and so to a more uniform intensity distribution within the azimuthal course of the Debye-Scherrer rings.

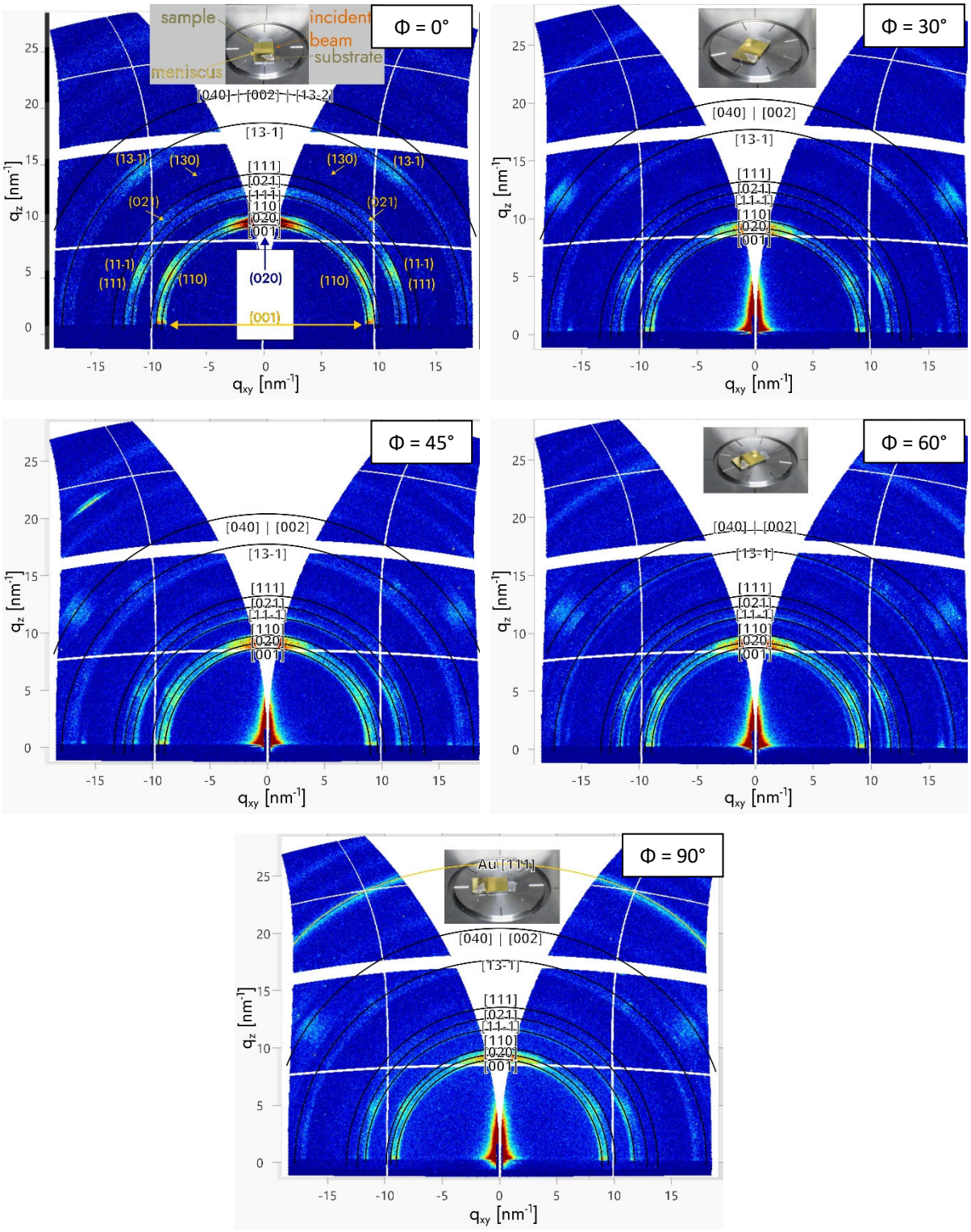

Figure 6: GIWAXS detector patterns for $[Rh_2(ac)_4(pyz)]_n$ with azimuthal rotation of the sample (100 deposition cycles): 0° (perpendicular to dipping direction), 30°, 45°, 60° and 90°.

AFM Evaluation of the $[Rh_2(ac)_4(pyz)]_n$ crystal growth

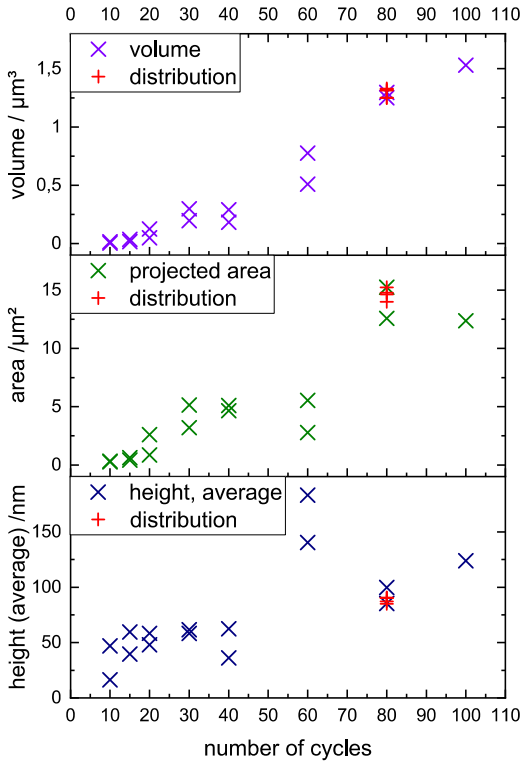

Figure 7: height, volume and coverage evaluation of the crystal growth of $[Rh_2(ac)_4(pyz)]_n$ versus the number of deposition cycles applied.

For the evaluation of the crystal growth, the AFM pictures were analyzed using the particle size analysis tool of the Gwyddion software.[4] The average height, volume, and packing density was calculated for different numbers of applied cycles. Every evaluation was carried out for two different samples after same the same number of cycles have been applied. For a low number of cycles, the scattering of the values is higher than for large numbers of cycles applied. This effect is caused by a less quantity of crystals in the AFM picture. For a better clarification the distribution of the parameters was shown for the sample after 80 cycles. Five random positions at the same sample surface were therefore evaluated. Within one sample the differences were smaller in comparison to the differences between two samples with the same coating.

AFM fine structure investigation of crystal surface

One of the well-shaped $[Rh_2(ac)_4(pyz)]_n$ crystals was further investigated by AFM to determine the fine structure of the crystal surface. In the resulting picture in Figure 8 shows a terraces structure. The individual steps can be related to the crystal growth by the step height. The profile of line 1 indicates an equivalent step height.

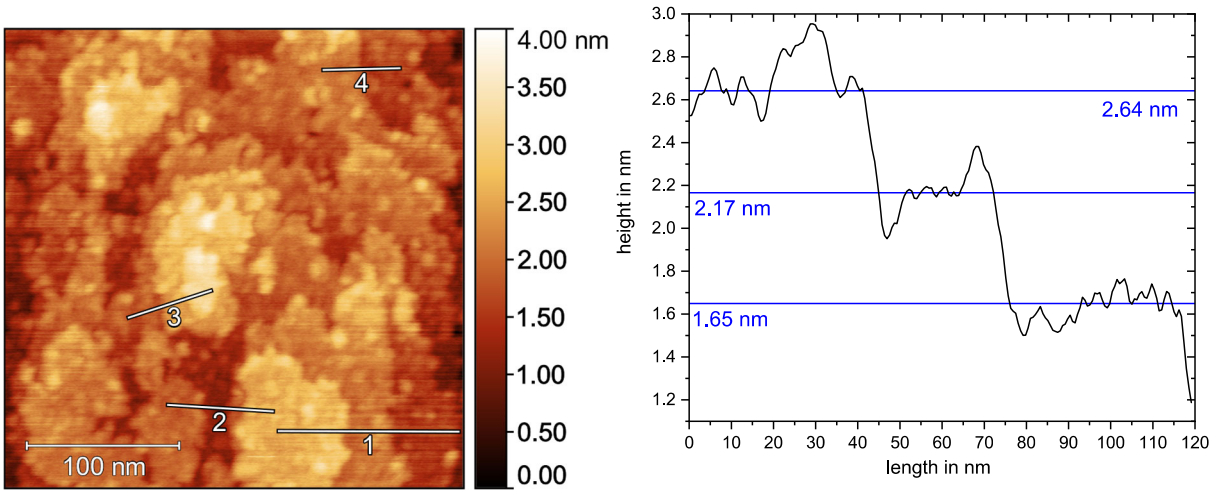

Figure 8: left: detailed AFM picture (0.3 µm x 0.3 µm) of a crystal surface of $[Rh_2(ac)_4(pyz)]_n$ after 80 cycles; right: line profile 1.

The Gwyddion software was used to obtain a histogram of the heights and a compilation of the edge heights. These three methods were used to obtain the step height as it is shown in Figure 9. The median is determined between 0.50 nm and 0.65 nm which is near the theoretical height of 0.72 nm of one crystal cell. Also, a single paddle-wheel complex with 0.47 nm (0.49 nm with a bonded pyrazine) is in the range of the observed heights.

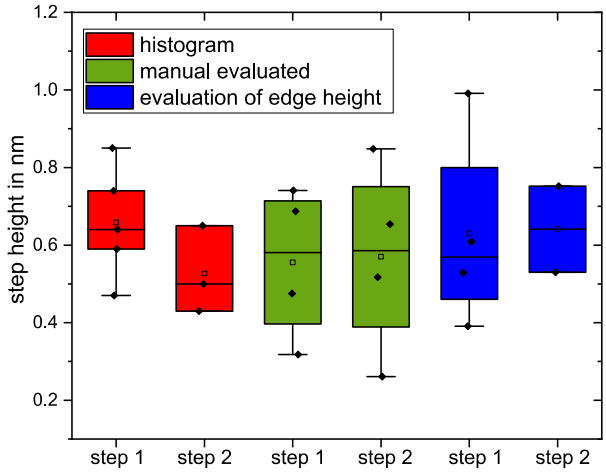

Figure 9: step height in comparison of different methods.

EDX investigation

The energy-dispersive X-ray spectroscopy (EDX) measurements were done with an FEI Quattro SEM and an EDAX octane plus detector at 20 kV. In Figure 10 four measurement spots are mentioned. Each spot was measured for 30 seconds with an amp time of 1.92 µs and a detector resolution of 135.1 eV. Spots 1 and 3 refer to the crystal-free gold surface and the spots 2 and 4 to crystals standing, respectively lying on the surface.

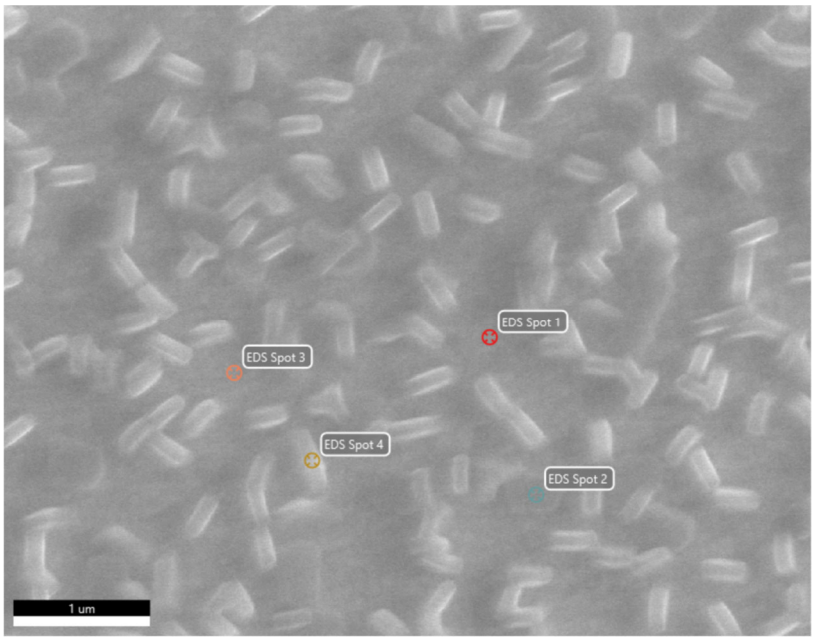

Figure 10: investigation spots for EDX measurement of $[Rh_2(ac)_4(pyz)]_n$ after 60 cycles, 30000x magnification

In the spectrum, the elements C, N, O, Al, Si, Al, S, Ti, Au and Rh were detected. Si, Ti and Au are part of the wafer and the coated surface. C, N, O and Rh are part of the crystals. Al must be a pollution and is not further considered.

Spot	**uncovered gold surface**		**crystals**	
	1 **[weight %] (Error)**	**3** **[weight %] (Error)**	**2** **[weight %] (Error)**	**4** **[weight %] (Error)**
C	8.7 (±1.8)	8.6 (±1.7)	15.6 (±2.4)	16.1 (±2.4)
N	0.8 (±0.8)	1.2 (±1.1)	2.1 (±1.0)	1.0 (±1.0)
O	1.2 (±0.4)	1.3 (±0.4)	2.6 (±0.5)	2.2 (±0.4)
Rh	0.3 (±0.2)	0.4 (±0.2)	1.9 (±0.4)	1.6 (±0.3)
S	0.7 (±0.1)	0.7 (±0.1)	0.6 (±0.1)	0.6 (±0.1)
Au	70.4 (±4.2)	70.6 (±4.0)	62.3 (±3.9)	63.2 (±3.9)

Even though the light elements C, N and O have a high error, a trend between the uncovered surface and the crystals is visible. The difference in the amount of carbon is the most remarkable thing beside the higher rhodium content at spots covered with crystals. The amount of sulphur is within the limits of the errors similar across all considered locations. So, it can be assumed that the SAM is covering the surface completely. The slightly smaller ratio

of sulphur at crystal spots is probably connected to an absorption of x-rays on their path from the surface through the crystal.

Anisotropy determination

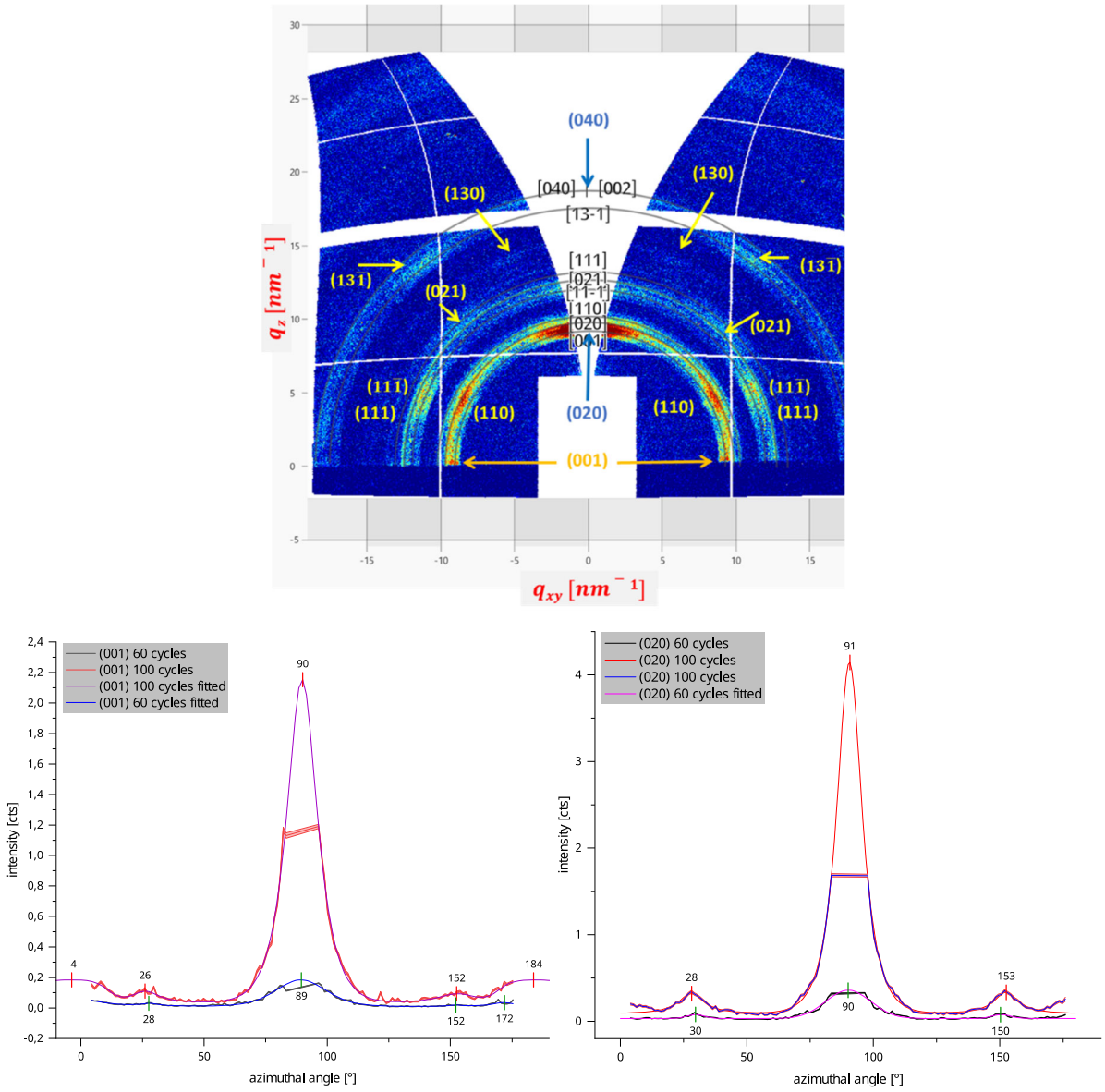

Figure 11: Azimuthal line scan for anisotropy determination along the (001) (bottom left) and (020) (bottom right) reflection of $[Rh_2(ac)4(pyz)]_n$ after 60 or 100 cycles (bottom; q_z against q_{xy}; masked central area was interpolated by help of Gauss-Lorentz fits), derived from GIWAXS pattern at 0.23° inclination angle (top; sample after 100 deposition cycles)

The last figure demonstrates the data extraction for the determination of the anisotropy factor according to Cinander and Burghardt.[5] The fitted curves were used for the calculation procedure.

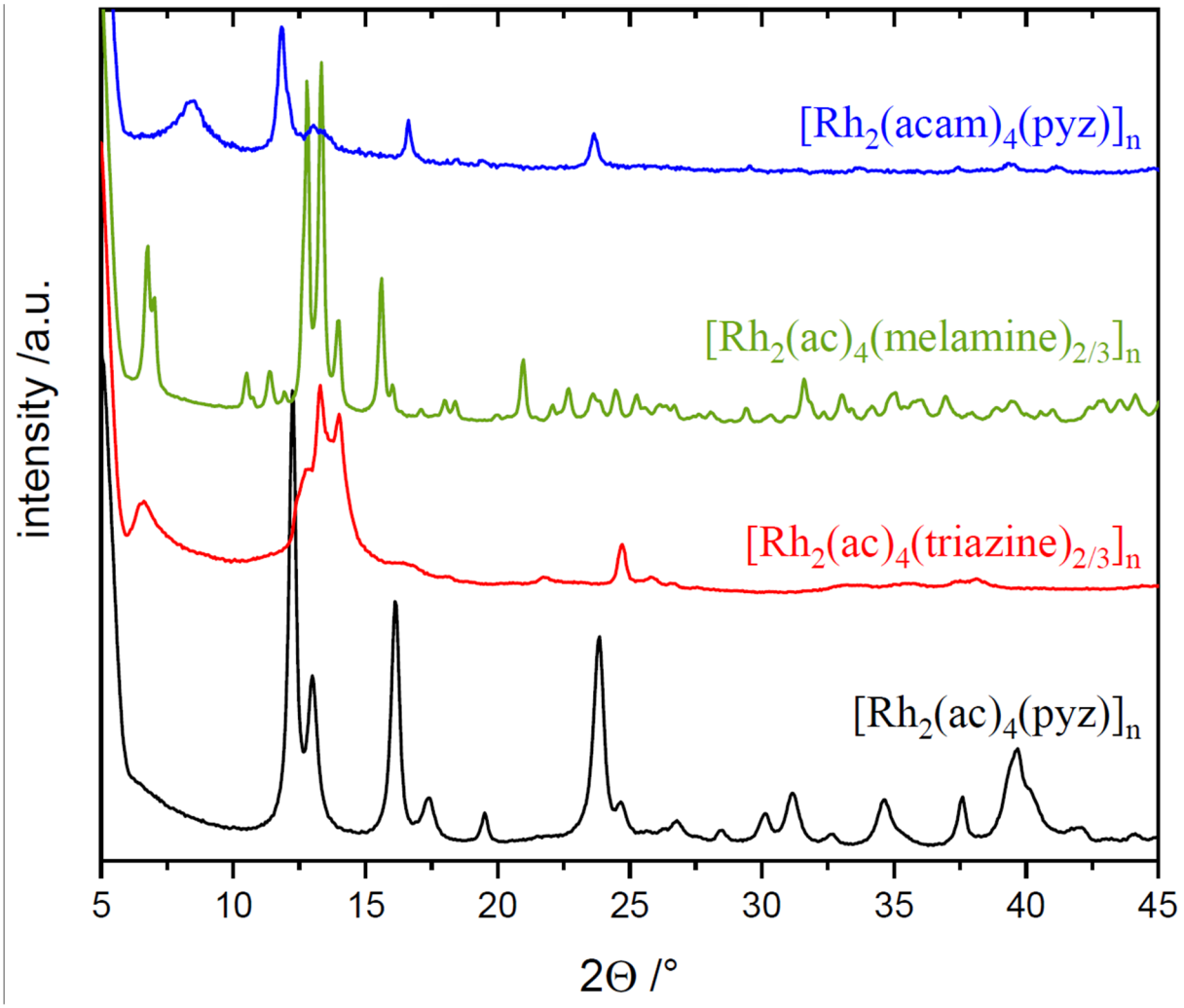

Figure 12: Powder-XRD data of all compounds discussed in the main document. In addition, the diffractogramme of the pyrazine-linked acetamide-based analogue of the acetate-based compound 1 ($[Rh_2(ac)_4(pyz)]_n$) (from Ref.[6]) was included for comparison purposes.

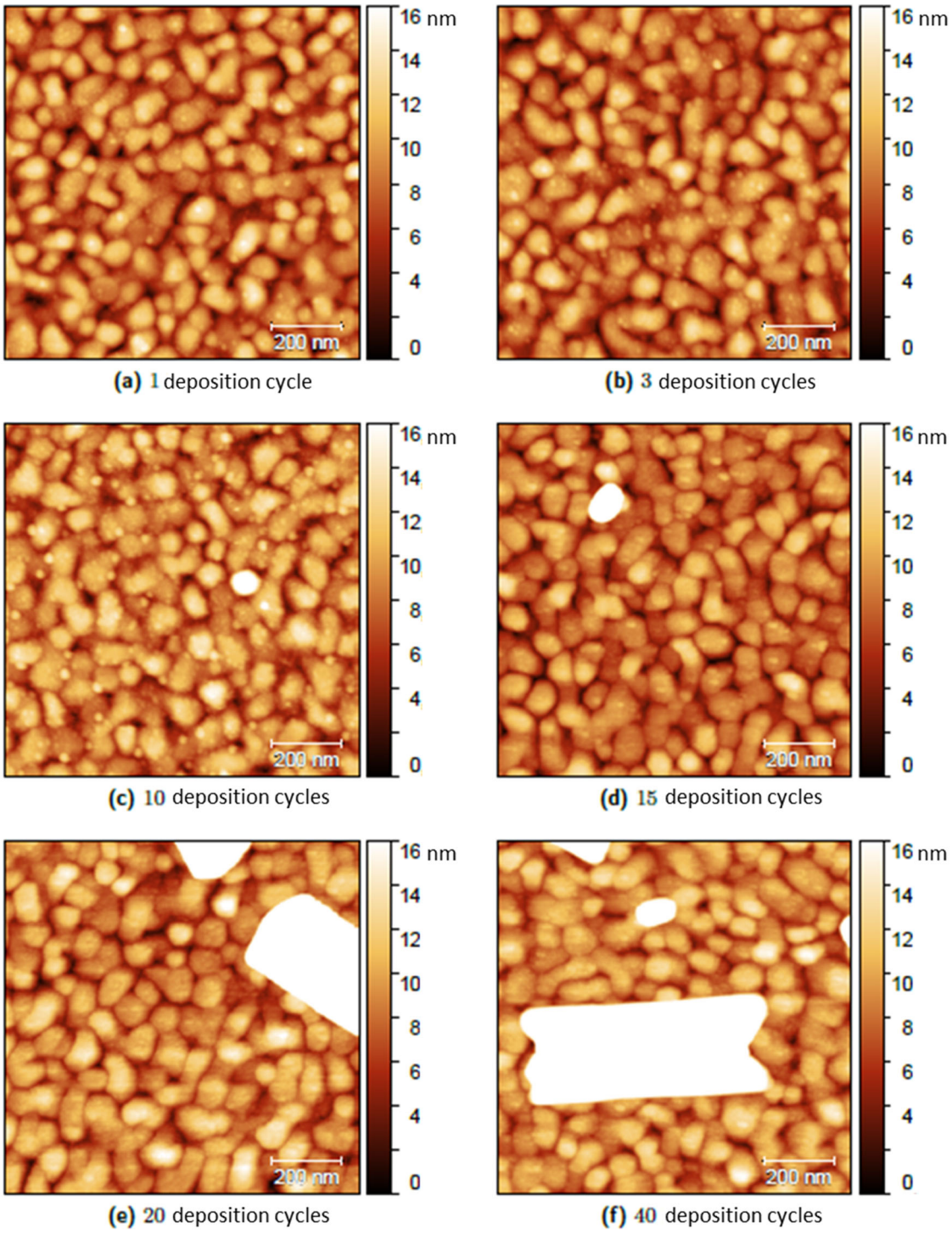

Figure 13: 1 µm x 1 µm AFM topographic images of $[Rh_2(ac)_4(pyz)]_n$-coated wafers. The height scale was fixed to 16 nm to trace the development of the small "nuclei".

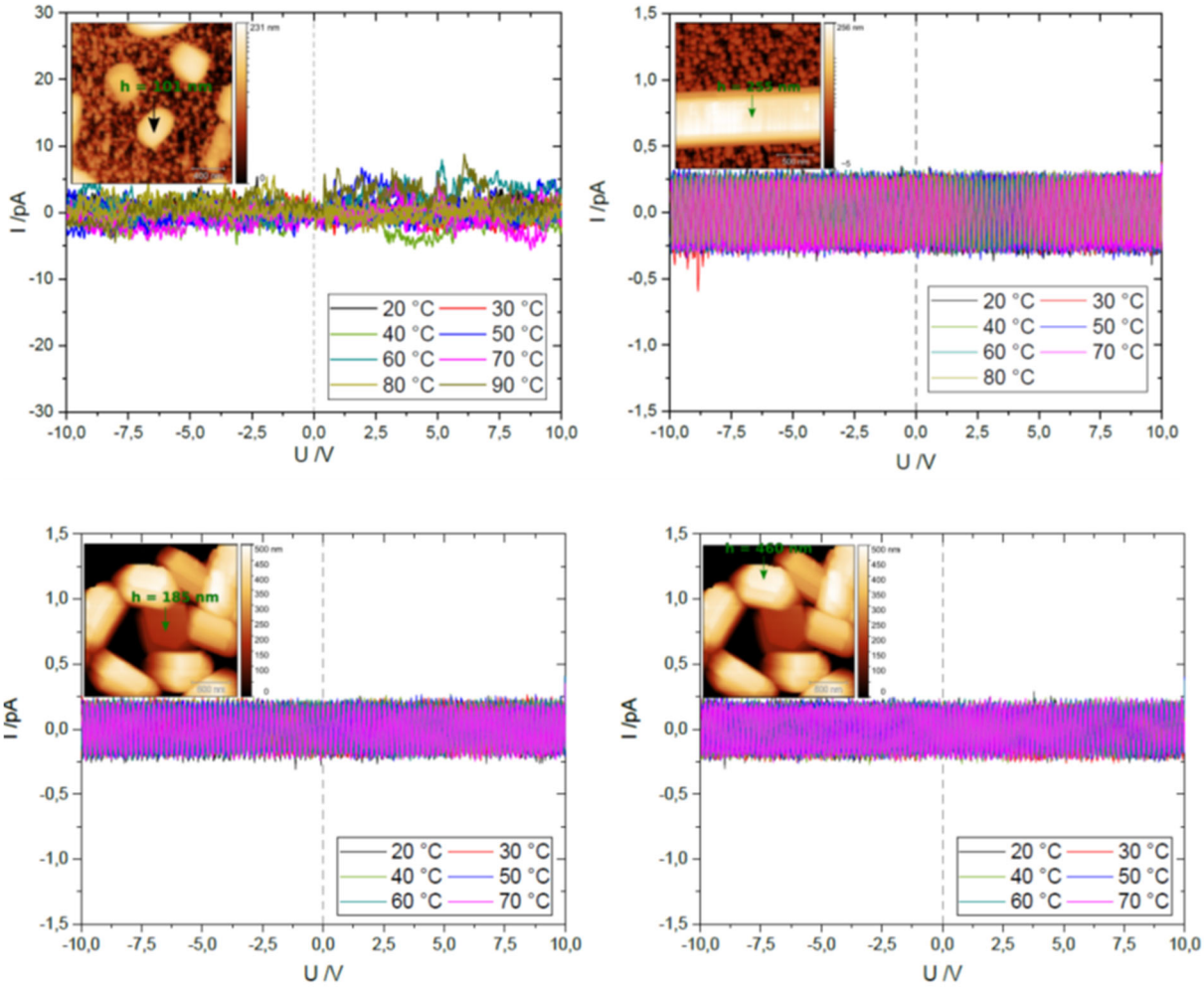

Figure 14: conductive-AFM (c-AFM) measurements of compound 1 (top left), 2 (bottom; both at standing and lying crystals) and 3 (top right)

Figure 14 illustrates the negligible conductivity of these acetate-based coordination polymers.

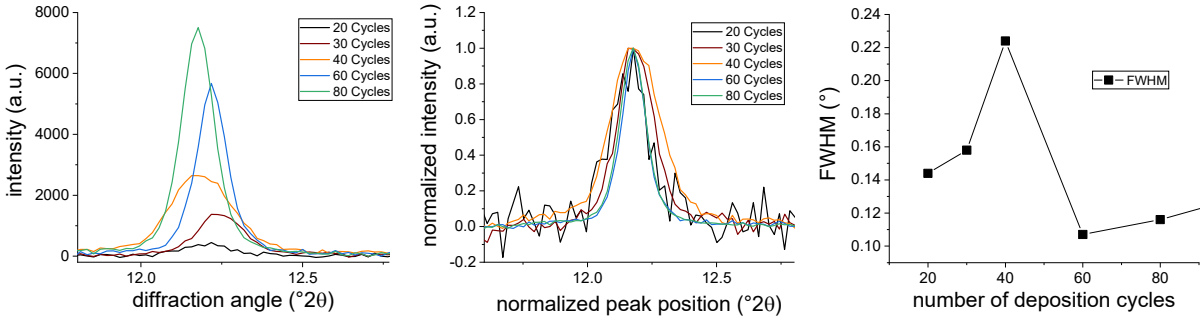

Figure 15: Main reflection of diffractogram (left; see main part; Fig. 5) of compound 1 in dependence of deposition cycles (middle: normalized representation; right: full width at half maximum FWHM for the main reflection)

Figure 15 shows the main reflection from Figure 5 (main part) in dependence of the deposition number. Interestingly, the peak location shifts slightly, which might be a consequence of different contributions to the main peak caused by overlapping (001)/(020) reflections or by contributions of a slightly different crystal lattice for the lying crystals (see discussion in the main part). The full width at half maximum (FWHM) shows a maximum close to the deposition number, where a transition towards standing crystals was identified. This maximum points to a minimum average crystal size at the deposition number, where new standing crystals develop.

References:

[1] M. Tolan, *X-Ray Scattering from Soft-Matter Thin Films*. *Materials Science and Basic Research*, Springer Berlin / Heidelberg, Berlin, Heidelberg, **1999**.

[2] G. Pospelov, W. van Herck, J. Burle, J. M. Carmona Loaiza, C. Durniak, J. M. Fisher, M. Ganeva, D. Yurov, J. Wuttke, *Journal of Applied Crystallography* **2020**, *53*, 262.

[3] G. Renaud, R. Lazzari, F. Leroy, *Surface Science Reports* **2009**, *64*, 255.

[4] D. Necas, P. Klapetek, *Central European Journal of Physics* **2012**, *10*, 181.

[5] D. K. Cinader Jr., W. R. Burghardt, *Journal of Polymer Science, Part B: Polymer Physics* **1999**, *37*, 3411.

[6] D. Steinbach, S. Gersdorf, J. Heitmann, F. Mertens, *J. Phys. Chem. C* **2022**, *126*, 16421.